ISSN 0018-151X, High Temperature, 2013, Vol. 51, No. 1, pp. 97–105. © Pleiades Publishing, Ltd., 2013.
Original Russian Text © A.E. Galashev, O.R. Rakhmanova, 2013, published in Teplofizika Vysokikh Temperatur, 2013, Vol. 51, No. 1, pp. 105–114.

HEAT AND MASS TRANSFER AND PHYSICAL GASDYNAMICS

Temperature Changes of the Optical Properties of $(SiO_2)_n$, $(GaAs)_m$, and $(SiO_2)_n(GaAs)_m$ Nanoparticles: Computer Experiment

A. E. Galashev and O. R. Rakhmanova

Institute of Industrial Ecology, Ural Branch, Russian Academy of Sciences, Yekaterinburg

Received December 15, 2011

Abstract—The optical properties of silicon dioxide and gallium arsenide nanoparticles and the four-component particles based on them were calculated by the molecular dynamics method. The complex dielectric permittivity, infrared and Raman spectra, refractive index, and absorption coefficient of these nano particles were determined. The temperature dependences of the infrared and Raman spectra and the number of the optically active electrons in the nanoparticles composed of a semiconductor and/or a dielectric were investigated.

DOI: 10.1134/S0018151X1206003X

INTRODUCTION

Nanoparticles have typical colloidal properties. The most characteristic one is the high percentage of atoms occupying the nanoparticle surface. The surface atoms have unsaturated bonds and, hence, can bind to the other atoms; i.e., they have high chemical activity. The particle size, surface condition, and interatomic interaction specify the unique properties of nanoparticles and make potential application of them in many fields possible [1, 2].

Silicon dioxide is an essential material for technical application. It is used in optical and fiber devices and in microelectronics (e.g., metal-oxide semiconductor transistors). Silicon dioxide has many crystal forms: quartz, cristobalite, tridymite, and stishovite. But the best-known form is amorphous silicon dioxide. This form can be produced in the purest state. These forms of SiO_2 have SiO_4 as a base unit, where every Si atom is coordinated with four O atoms forming a tetrahedron, and every atom of oxygen serves as a bridge bonding two tetrahedrons. In various forms of SiO_2, the tetrahedrons are bonded in a variety of ways. This bonds in α-quartz and silicon dioxide are almost identical. In α-quartz the length of the bond Si–O is estimated at 1.61 Å and the angle Si–O–Si is estimated at 144°. In amorphous SiO_2 these two parameters have a random distribution but their average values are identical to that for α-quartz. In α-quartz, an almost perfect tetrahedron SiO_4 is stable and has only a small deviation of the angle from 109°. In amorphous SiO_2, the Si–O–Si-bonds range from 1.55 to 1.65 Å as the angle varies from 136° to 180°.

The amorphous GaAs has good optical and electronic properties. Considerable efforts go into producing the crystal GaAs. Nano-GaAs acquires new properties, opening up fresh opportunities for technical applications and widespread use of these materials. The GaAs films are deposited on various substrates, e.g., on Si. But for practical application, in many cases SiO_2 is more preferable as a substrate. For nanoparticles, the SiO_2 coating is more commonly deposited outside the particle. This considerably increases the thermal stability of the nanoparticle, due to the fact that the melting temperature of SiO_2 ranges from 1873 to 1998 K. The energy structure of the system InAs/InGaAs/GaAs is considered in [3]. The process of generating point and cluster defects both in the volume system of GaAs and in the thin films of GaAs was investigated in [4] by the molecular dynamics method. While irradiating GaAs with high-speed ions, most of the defects were shown to be generated near the ions, but the biggest cluster defects can be generated along the route of the bombarding ions. In [5], the heterostructure, obtained by depositing Ge on the substrate of GaAs, is considered as a precision material for manufacturing various detectors. The optical and dielectric properties of the nanoparticles of GaAs covered with SiO_2 have not been investigated to date, and the nanoparticles $(SiO_2)_n$ and $(GaAs)_m$ with inverted placement of components (GaAs is outside) were not produced. The molecular dynamic calculations [6–9] suggest that the Tersoff potential can adequately reproduce the physical properties of a multicomponent system.

Our main concern is investigating the infrared and Raman spectra of the nanoparticles $(SiO_2)_n$ and $(GaAs)_m$, the SiO_2-base being both inside and outside the nanoparticle, and specifying the frequency dependence of the refraction index η and the absorption coefficient κ of such nanoparticles in the temperature range of $300 \le T \le 1500$ K.

Tersoff potential parameters

Parameter	Silicon [8]	Oxygen [8]	Gallium [9]	Arsenic [9]
A, eV	1803.79	1882.55	2543.2972	1571.86084
B, eV	471.195	218.787	314.45966	546.4316579
λ_1, Å^{-1}	2.4799	4.17108	2.50842747	2.384132239
λ_2, Å^{-1}	1.7322	2.35692	1.490824	1.7287263
$R^{(1)}$, Å	2.5	2.7	3.4	3.4
$R^{(2)}$, Å	2.8	3.0	3.6	3.6
β	1.1×10^{-6}	1.1632×10^{-7}	0.23586237	0.00748809
n	0.78734	1.04968	3.4729041	0.60879133
h	–0.59825	–0.845922	7.1459174	0.15292354
c	1.0039×10^5	6.46921×10^4	0.07629773	5.273131
d	16.217	4.11127	19.796474	0.75102662
χ	1	1	1	1

COMPUTER MODEL

The potential of the Tersoff type has limited ability to reveal the differences in chemical interaction, but it defines the chemical differences of the valency s and p electron properties. This potential is an effective instrument for modeling new materials. The Tersoff potential is based on the concept of bond order. The interatomic potential energy of two neighboring atoms i and j is written as [6]

$$V_{ij} = f_C(r_{ij})\left[Aa_{ij}\exp\left(-\lambda^{(1)}r_{ij}\right) - \chi Bb_{ij}\exp\left(-\lambda^{(2)}r_{ij}\right)\right], \quad (1)$$

$$f_C(r_{ij}) = \begin{cases} 1, & r < R - D, \\ \frac{1}{2} - \frac{1}{2}\sin\left[\frac{\pi}{2}(r - R)/D\right], & R - D < r < R + D, \\ 0, & r > R + D, \end{cases} \quad (2)$$

where b_{ij} is the many-particle parameter of bond order (3), specifying the creation of bonding energy (the attractive part of V_{ij}) in the case of local atom distribution in the presence of other neighboring atoms (k-atoms). The potential energy is a many-particle function of positions of the atoms i, j, and k, and it is influenced by the parameters

$$b_{ij} = \left(1 + \xi_{ij}^{n_i}\right)^{-1/(2n)}, \quad (3)$$

$$\xi_{ij} = \sum_{k \neq i,j} f_C(r_{ij})\beta_i g(\theta_{ijk})\exp\left[\lambda_3^3(r_{ij} - r_{ik})^3\right], \quad (4)$$

$$g(\theta) = 1 + \frac{c^2}{d^2} - \frac{c^2}{\left[d^2 + (h - \cos\theta)^2\right]}, \quad (5)$$

$$a_{ij} = \left(1 + \alpha^n \eta_{ij}^{n_i}\right)^{-1/(2n)}, \quad (6)$$

$$\eta_{ij} = \sum_{k \neq i,j} f_c(r_{ij})\exp\left[\lambda_3^3(r_{ij} - r_{ik})^3\right], \quad (7)$$

$$\lambda_{ij}^{(k)} = \left(\lambda_i^{(k)} + \lambda_j^{(k)}\right)/2, \quad A_{ij} = (A_i A_j)^{1/2}, \quad B_{ij} = (B_i B_j)^{1/2},$$

$$R^{(1)} = R - D, \quad R^{(2)} = R + D,$$

$$R_{ij}^{(1)} = \left(R_i^{(1)} R_j^{(1)}\right)^{1/2}, \quad R_{ij}^{(2)} = \left(R_i^{(2)} R_j^{(2)}\right)^{1/2},$$

where ξ is the effective coordination number; $g(\theta)$ is the function of the angle between r_{ij} and r_{ik}, that stabilizes the tetrahedral structure; λ_3 and α are set equal to zero.

The potential defined by Eqs. (1)–(7) is differentiated from the corresponding potential of the single-component system [7] by introducing one additional parameter χ. This parameter amplifies or attenuates the heteropolar bonds with respect to the value obtained by simple interpolation. Thus, the "chemistry" is involved in this parameter or it is taken into account on choosing the interpolation formula. Here, $\chi_{ii} = 1$ and $\chi_{ij} = \chi_{ji}$, so only one independent parameter is required for a pair of two atom types. The parameter β in Eq. (4) is involved for getting additional flexibility, which is typical for the pair made up of the atoms of essentially different types.

The parameters of the Tersoff potentials for silicon, oxygen, gallium, and arsenic are tabulated in the table [8, 9]. Here, the deficiently physically justified parameter χ_{ij} is assumed equal to one. The procedure of adjusting parameters with using the original Tersoff potential is presented in [10]. The Tersoff potential is well transferable for the bond orbitals; the parameters fitted for sp^3-hybridization can be used for the description of interaction in the materials with sp^2-hybridization [11].

The initial configurations of nanoparticles were made by cutting the spheres and spherical layers out of the crystal of GaAs with the structure of zinc blende and the crystal of α-quartz. The previously built crys-

tal of GaAs was specified by the parameter of the cubic lattice: $a = 0.5653$ nm [12]. The packing of SiO_4-tetrahedrons for obtaining the crystal of α-quartz with the parameters a, $b = 0.5082$ nm, $c = 0.55278$ nm [7] was generated by the program-generator of mineral crystal structures GRINSP [13]. The four-component particle was built by surrounding a sphere consisting of one type of base units by a layer of the other atomic units. In order to obtain the nanoparticles of the first type, a sphere of SiO_2 was inserted into the spherical layer of GaAs, aligning their centers. Producing the nanoparticle of the second type included analogous attachment of the sphere of GaAs to the spherical layer of SiO_2. In both cases, in the region of interfacing the sphere and the layer surrounding it, the base units of the spherical layer, the atoms of which were closer to any atom of the sphere than a certain selected value r_m, were removed. As a result, after assembling the nanoparticles, the minimal spacing between the atoms of different types ranged between 0.33 and 0.36 nm. The required quantity of base units of each type remained outside in the vicinity, while the atoms located farther than the others from the center of mass of the created nanoparticle were removed. Finally, depending on its composition, the nanoparticle contained 86 base units of SiO_2, or 129 base units of GaAs, or 50 base units of SiO_2 and 54 base units of GaAs. In other words, in every case the nanoparticle was generated from 258 atoms. The calculation of physical properties was performed by the classical molecular-dynamic ensemble representing the special case of a microcanonical ensemble. Integration of the equations of motion was performed by the Runge–Kutta method of the 4th order with the time step $\Delta t = 10^{-16}$ s. In the preliminary stage of calculation with duration of $100000\Delta t$, the correction of the velocities of atoms was performed in order to balance the systems at a given temperature. The major calculation was made without any correction and lasted for 10^6 time steps. The molecular-dynamic (MD) calculations for every nanoparticle, I $(SiO_2)_{86}$, II $(GaAs)_{129}$, $(SiO_2)_{50}(GaAs)_{54}$ with interior (III) and surface (IV) placement of SiO_2, were performed for three temperature values (300, 900, and 1500 K). The configurations of the nanoparticles, produced at low temperatures, were used in the calculations at higher temperatures.

DIELECTRIC PROPERTIES

The calculation of the dielectric properties of the nanoparticles of silicon dioxide and gallium arsenide and the four-component particles based on them differs from the calculation of the corresponding characteristics of oxygen- and ozone-containing water clusters in the presence of the ions $\left(Br^-\right.$ and $\left.NO_3^-\right)$ [14–17]. The water or ozone (oxygen) molecule invariant in composition acts as a base unit for the water systems. Each molecule has its own electrical characteristics: permanent dipole moment $\mathbf{d}^{\text{per}}$, polarizability $\alpha^{(p)}$, and calculated induced dipole moment $\mathbf{d}^{\text{ind}}$. The compositionally stable molecules can be found neither in silicon dioxide nor in gallium arsenide nor in the nanoparticle based on them. Consequently, in this case the exact characteristics of molecules ($\mathbf{d}^{\text{per}}$, $\alpha^{(p)}$, and $\mathbf{d}^{\text{ind}}$) cannot be used for calculating the dielectric properties of nanoparticles. But the presence of covalent bonds in SiO_2 and GaAs or their combination $(SiO_2)_n(GaAs)_m$ makes it possible to isolate the local units from some atom, surrounded by any other atoms of a nanoparticle, at each instant of time. The number of neighbors of every atom is chosen according to the assumed parameters of the interaction potential and does not exceed four, as a rule. The experimental values of polarizability were taken as 3.75, 0.793, 8.1, and 4.3 Å^3 [18] for the atoms of Si, O, Ga, and As, respectively. The permanent dipole moments of these atoms were assumed equal to zero. Considering the individual characteristics of atoms $\mathbf{d}^{\text{per}}_{\text{atom}}$ and $\alpha^{(p)}_{\text{atom}}$, one can determine the effective values of these quantities and $\mathbf{d}^{\text{ind}}$ for the local groups of atoms. Precisely these effective characteristics of the local groups of atoms were used for calculating the dielectric properties of the nanoparticles $(SiO_2)_{86}$, $(GaAs)_{129}$, and $(SiO_2)_{50}(GaAs)_{54}$.

The dielectric permittivity $\varepsilon(\omega)$ as a frequency ω function was presented by the complex value $\varepsilon(\omega) = \varepsilon'(\omega) - i\varepsilon''(\omega)$, For determining this value, the following equation was used [14, 15]:

$$\frac{\varepsilon(\omega)-1}{\varepsilon_0-1} = -\int_0^\infty \exp(-i\omega t)\frac{dF}{dt}dt = 1 - i\omega\int_0^\infty \exp(-i\omega t)F(t)dt,$$

where ε_0 is the static dielectric permittivity, $F(t)$ is the normalized autocorrelation function of the total dipole moment of a nanoparticle:

$$F(t) = \frac{\langle \mathbf{M}(t)\cdot\mathbf{M}(0)\rangle}{\langle \mathbf{M}^2\rangle},$$

where

$$\mathbf{M}(t) = \sum_{j=1}^{N}\mathbf{d}_j(t)$$

is the sum of the total dipole moments of the atoms. Calculating the values $\mathbf{d}_j = \mathbf{d}_j^{\text{per}} + \mathbf{d}_j^{\text{ind}}$, for each atom, only those neighbors that interacted with this atom according to the potentials in use were taken into account.

The Raman and infrared (IR) spectra of nanoparticles were calculated by the autocorrelation functions of fluctuations of the polarizability and dipole moment, respectively. The dipole moment $\mathbf{d}_i$ and polarizability $\boldsymbol{\alpha}_i$ of i-th atom are formed due to the

interaction with the surrounding atoms, and as a result, we get [16, 17]

$$\begin{aligned}\mathbf{d}_i &= \mathbf{d}_{i,0} + \boldsymbol{\alpha}_{i,0}\sum_{j\neq i}\mathbf{T}_{ij}\mathbf{d}_j,\\ \boldsymbol{\alpha}_i &= \boldsymbol{\alpha}_{i,0} + \boldsymbol{\alpha}_{i,0}\sum_{j\neq i}\mathbf{T}_{ij}\boldsymbol{\alpha}_j,\end{aligned} \quad (8)$$

where $\mathbf{d}_{i,0}$ and $\boldsymbol{\alpha}_{i,0}$ are the dipole moment and polarizability gained by an atom i before interaction with the renewed (as a result of temperature motion) surroundings.

Here, $\mathbf{T}_{ij}$ is the tensor of dipole–dipole interaction

$$\mathbf{T}_{ij} = \frac{1}{|r_{ij}|^3}\left(3\hat{\mathbf{r}}_{ij}\hat{\mathbf{r}}_{ij} - \mathbf{1}\right),$$

where $\mathbf{r}_{ij}$ is the unit vector having the direction $\mathbf{r}_i - \mathbf{r}_j$, $\mathbf{r}_i$ and $\mathbf{r}_j$ are the positions of the centers of atoms i and j, and $\mathbf{1}$ is the unit tensor of rank 3 × 3. The system of equations (8) was solved by the iteration method.

The scattering cross section of infrared emission was defined by the equation [19]

$$\sigma(\omega) = \left(\frac{2}{\varepsilon_v c\hbar\eta}\right)\omega\,\mathrm{th}\left(\frac{\hbar\omega}{2kT}\right)\mathrm{Re}\left(\int_0^\infty dt e^{i\omega t}\left\langle \mathbf{M}(t)\cdot\mathbf{M}(0)\right\rangle\right),$$

where η is the refractive index independent of frequency, ε_v is the dielectric permittivity of a vacuum, and c is the speed of light.

The scattered light frequencies are combinations of the exciting light frequency and the vibrational and rotational frequencies of molecules. The Raman scattering spectrum consists of the system of satellites, symmetrical with frequency ω with respect to the exciting line. The satellite with frequency $\omega - \omega_k$ (red, or Stokes, satellite) corresponds to the satellite with frequency $\omega + \omega_k$ (violet, or anti-Stokes, satellite). The Raman spectra arise in the transition of a molecule from the unexited vibrational state, specified by the vibrational quantum number $\nu = 0$, into the exited vibrational state with $\nu = 1$, 2, etc. Thus, measuring the frequencies of Raman scattering lines, one can determine the frequencies of natural (or normal) oscillations of a molecule, which appear in the Raman spectrum. At ordinary temperatures, the Stokes lines are much more intensive than the anti-Stokes lines because most of the molecules are in an unexcited state; as the temperature increases, the intensity of anti-Stokes lines rises due to partial thermal filling of excited vibrational states. The intensity of the Stokes satellites almost does not depend on temperature. The frequencies $\omega' = \omega - \omega_k$ and $\omega'' = \omega + \omega_k$, which do not depend on the incident light frequency, characterize the matter composition and structure. The number of satellites also depends on the scattering material. In the case of Stokes Raman scattering, the relationship between the energies of the incident and scattered photons takes the form

$$\hbar\omega' = \hbar\omega - \hbar\omega_k,$$

and in the case of anti-Stokes Raman scattering

$$\hbar\omega'' = \hbar\omega + \hbar\omega_k,$$

the term $\hbar\omega_k$ is the energy of an excited vibrational (or rotational) state of a molecule. In the Raman spectra, there are the overtones defined by the condition $\Delta\nu > 1$. Disregarding anharmonicity, these overtones are combinations of the exciting frequency and the frequencies multiple of ω_k ($2\omega_k$, $3\omega_k$, etc.).

The light being depolarized, the Raman spectrum is defined by the following equation [19]:

$$J(\omega) = \frac{\omega}{(\omega_L - \omega)^4}\left(1 - e^{-\hbar\omega/k_B T}\right)\mathrm{Re}\left(\int_0^\infty dt e^{i\omega t}\left\langle \Pi_{xz}(t)\Pi_{xz}(0)\right\rangle\right),$$

where

$$\Pi(t) \equiv \sum_{j=1}^{N}\left[\boldsymbol{\alpha}_j(t) - \left\langle\boldsymbol{\alpha}_j\right\rangle\right],$$

ω_L is the exciting laser frequency, Π_{xz} is the xz-component of $\Pi(t)$, and the axis x is directed along the dipole of the group of directly interacting atoms (atom j and the neighbors interacting with it).

The refraction index η and the absorption coefficient ξ are defined by the equations [20]

$$\eta = \sqrt{\frac{\varepsilon' + \sqrt{\varepsilon'^2 + \varepsilon''^2}}{2}}, \quad \xi = \sqrt{\frac{-\varepsilon' + \sqrt{\varepsilon'^2 + \varepsilon''^2}}{2}}.$$

The coefficient ξ determines the rate of wave attenuation as it propagates in the medium.

The total number of electrons n_{el} interacting with the external electromagnetic field in a unit volume of the nanoparticle is defined by the following equation [20]:

$$n_{el} = \frac{m}{2\pi^2 e^2}\int_0^\infty \omega\varepsilon''(\omega)d\omega,$$

where e and m are the electron charge and mass.

RESULTS

The configurations of four nanoparticles obtained at $T = 1500$ K after 10^6 time steps are presented in Fig. 1. The island of oxygen atoms appeared in the top piece of nanoparticle $(SiO_2)_{86}$ at the surface. The surface of nanoparticle $(GaAs)_{129}$ is slightly disordered. The four-component nanoparticle with the core of SiO_2 still remains sufficiently compact, but the delamination of atoms Ga and As is observed at the surface. The nanoparticle with inverted arrangement of the SiO_2-component at the surface is characterized by the most loose, heterogeneous structure. In the dense central part of this nanoparticle, the bigger atoms of As dominate at the surface. The partially delaminated shell of

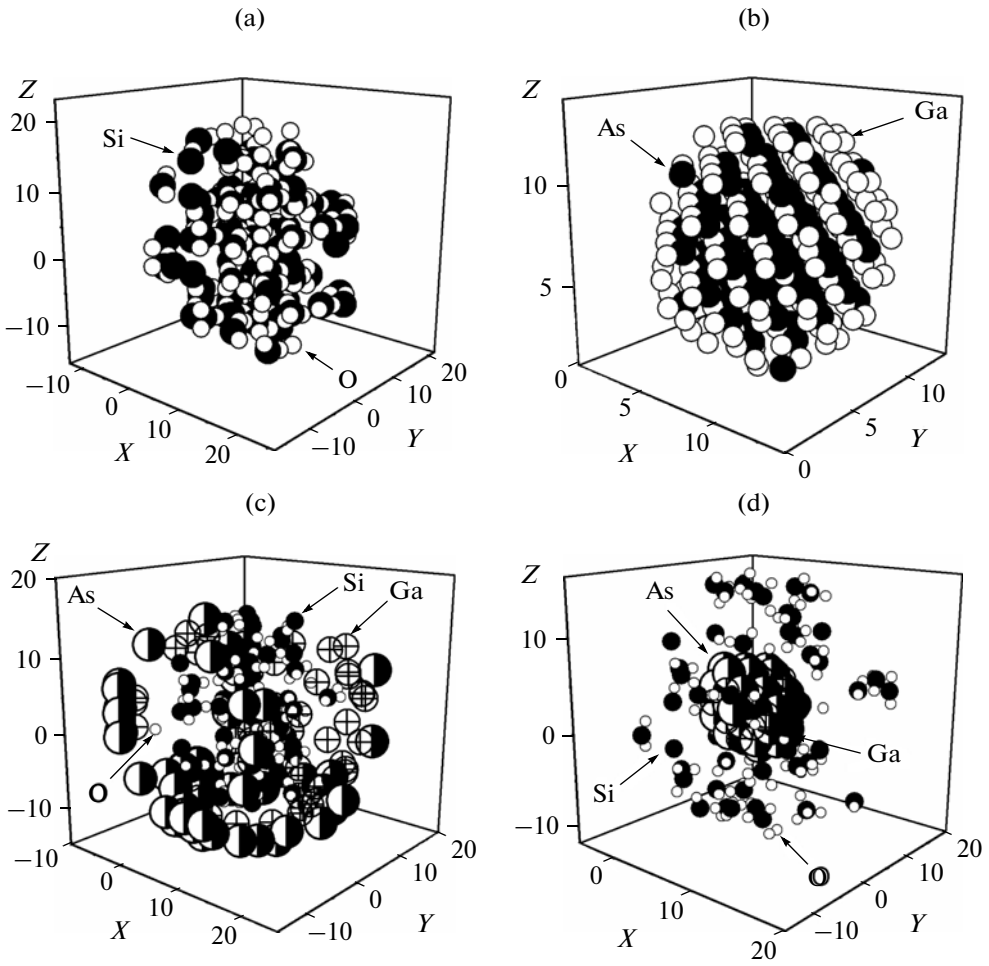

Fig. 1. Configurations of nanoparticles. (a) $(SiO_2)_{86}$; (b) $(GaAs)_{129}$; (c), (d) $(SiO_2)_{50}(GaAs)_{54}$: (c) SiO_2 inside, (d) SiO_2 outside the nanoparticle. The coordinates of atoms are given in Å.

SiO_2 is unequal in thickness and does not cover the GaAs core completely. The base units of SiO_2 do not all persist. In the surface region there are single atoms of Si and O and the base units, which are not connected to the frame: SiO, SiO_2, and SiO_4.

Let us consider the general properties of the nanoparticles at the temperature of 300 K, at which the spectral characteristics of GaAs and SiO_2 films and crystals are usually obtained. In most of the frequency range, the functions $\varepsilon'(\omega)$ and $\varepsilon''(\omega)$ are increasing; i.e., the dielectric response is enhanced with the increase in the outer radiation frequency (Fig. 2). For the nanoparticles $(SiO_2)_{50}(GaAs)_{54}$ of like composition but with different component placement (*1*, III; *2*, IV), the behavior of the frequency dependence of the real ε' and imaginary ε'' components of the dielectric permittivity at $T = 300$ K is rather identical. The values of function $\varepsilon'(\omega)$ for nanoparticles III and IV are enclosed by the experimentally obtained values of the corresponding functions for amorphous SiO_2 (curve *3*) [21] and the crystal of GaAs with the structure of zinc blende (curve *4*) [22]. At high frequencies the smoothing of oscillations of function $\varepsilon''(\omega)$ for particle III is observed.

The infrared absorption spectra of nanoparticles III and IV essentially differ in their intensity (*1*, III, *2*, IV, Fig. 3). The intensity of the infrared spectra of the nanoparticles under consideration is mostly caused by oscillations of atoms along the ion-covalent Si–O bonds. The locations of the peaks, which can be recognized for particle IV in the second, more high-frequency half of the spectrum $\sigma(\omega)$, coincide with the ones for particle III. The experimental infrared spectrum of the GaAs film [23] has fundamental peaks in the low-frequency half of the range under consideration ($0 \le \omega \le 1600$ cm^{-1}), and the major peak of the infrared spectrum of α-quartz [24] is located in the second (more high-frequency) half of this band.

In Fig. 4 are shown the infrared absorption spectra of nanoparticles III and IV, smoothed by the polynomial of the ninth degree and calculated for three temperatures. For nanoparticle III with the SiO_2-core, the

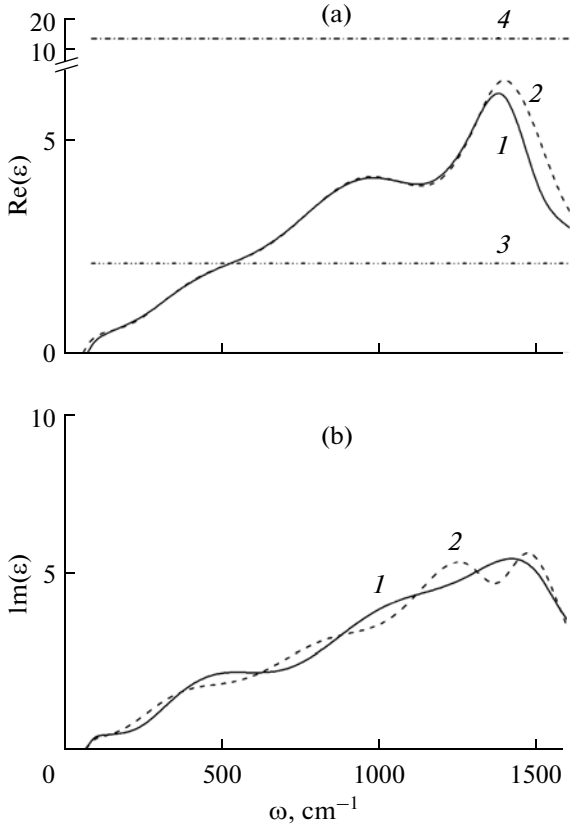

Fig. 2. The frequency dependence of real (a) and imaginary (b) components of dielectric permittivity for nanoparticles $(SiO_2)_{50}(GaAs)_{54}$: *1*, III; *2*, IV; *3*, amorphous SiO_2, experiment [21]; *4*, crystal GaAs, experiment [22].

intensity of σ(ω)-spectra I_{tot} decreases as the temperature rises (Fig. 4a). The relationship between the values of I_{tot} for temperatures 300, 900, and 1500 K is 1 : 0.85 : 0.49. Temperature variation does not lead to shifting of the fundamental peak (on 1380 cm^{-1}) of the σ(ω)-spectra. The decrease in the infrared spectrum intensity with increasing temperature is caused by intensification of attenuation of the autocorrelation function of the total dipole moment. The faster attenuation of this function at high temperature is provided both by decreasing the value of $|\mathbf{M}|$ and faster change of the vector $\mathbf{M}$ direction. But the continuity of decreasing the σ(ω)-spectrum intensity with increasing temperature is broken in the case of nanoparticle IV with external placement of the SiO_2 component. This is due to the weak impact of the GaAs-core on the outer shell of SiO_2 at $T = 300$ K. At 900 K the loose structure of SiO_2 consolidates because the atoms of Si and O approach the GaAs core consisting of heavier atoms. As this takes place, the distance between Si and O atoms reduces. This amplifies the Si- and O-atom oscillations. As a result, the σ(ω)-spectrum intensity significantly increases. As temperature further rises (up to 1500 K), the nanoparticle with a more homogenous structure behaves naturally: the infrared spectrum intensity decreases due to reducing the correlation time of the total dipole moment. The relationship between the I_{tot} values for nanoparticle IV when passing from 300 K to 900 and 1500 K is 1 : 1.80 : 0.76.

The anti-Stokes Raman spectra $J(\omega)$ for nanoparticles III and IV essentially differ from each other not in intensity but in the number and location of peaks. In the frequency range being studied, there are observed five Raman shifts (peaks at $\omega > 0$) for nanoparticle IV and four distinguished frequency shifts for particle III (Fig. 5). The experimental Raman spectrum of GaAs

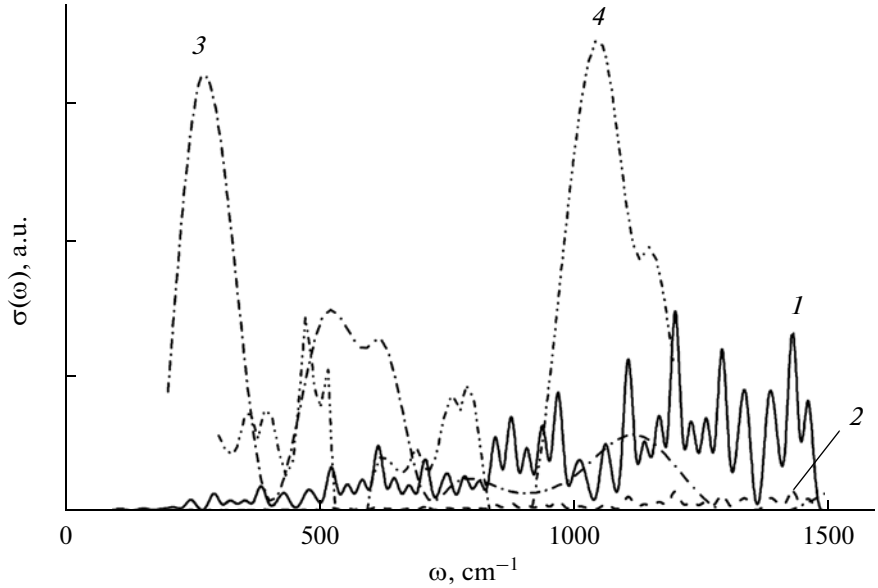

Fig. 3. The infrared absorption spectra for various systems: *1*, nanoparticle III; *2*, nanoparticle IV; *3*, amorphous gallium, experiment [23]; *4*, α-quartz, experiment [24].

film at $T = 300$ K (curve *3*) was obtained up to $\omega < 700$ cm^{-1} and had two fundamental bands on the frequencies of ~60 and 230 cm^{-1} [23]. These bands characterize the acoustic and optical vibrational modes of amorphous GaAs,respectively. One should note that the band 245 cm^{-1}, which is likely to be caused by the optical mode of crystal GaAs, is present in the Raman spectrum of nanoparticle IV. The Raman spectrum of nanoparticle IV differs significantly from the corresponding spectrum of nanoparticle III. Recall that in this case GaAs in the nanoparticle is a compact nanocrystal. The peak with weak intensity on $\omega = 1450$ cm^{-1} in the $J(\omega)$-spectrum of nanoparticle III can be considered as an overtone of the second mode (422 cm^{-1}) to a precision of 13%. The fundamental peaks of the Raman spectrum of α-quartz (curve *4*) [24] and molten quartz (curve *5*) [25] are located at the frequencies of 437 and 463 cm^{-1}, respectively, which is in good agreement with the location of the Raman shift on 422 cm^{-1} for nanoparticle III with the center of the monolithic nanoparticle of SiO_2.

The temperature distinctions of the anti-Stokes Raman spectra of nanoparticles III and IV are obvious from Fig. 6. For both nanoparticles, the Raman spectrum intensity considerably increases as the temperature rises. This is due to retarding the attenuation of the autocorrelation function of fluctuations of atomic polarizability. As the temperature rises, the polarizability deviation from the mean and the correlation time of these functions increase. The first peak of the $J(\omega)$-spectrum of nanoparticles III and IV at $T = 300$ K is located in the range of $30 \le \omega \le 600$ cm^{-1}. At $T =$ 1500 K the first peak of nanoparticle IV keeps its location, while for nanoparticle III this peak has a blue shift by ~60 cm^{-1}. In [26] the Raman peak at the frequency of 47 cm^{-1} was generated due to the buffer layer of GaAs, obtained by the low-temperature molecular beam epitaxy. Such a low oscillation frequency was assigned to the presence of point defects (vacancies and interstitial atoms). Such defects can be generated, for example, as a result of excess of arsenic atoms and deficiency of gallium atoms. The intensity ratio $\left(J^{(2)}_{1500\,\mathrm{K}} \Big/ J^{(2)}_{300\,\mathrm{K}}\right)$ of the second peaks of $J(\omega)$-spectrum is 134.78 for nanoparticle III and 11.44 for nanoparticle IV. The location of the second peak (422 cm^{-1}) of $J(\omega)$-spectrum of nanoparticle III does not change as the temperature rises (Fig. 6a). However, the third peak has a red shift by 18 cm^{-1} at 1500 K. Peaks 2–5 of the $J(\omega)$-spectrum of particle IV do not shift under heating from 300 to 1500 K (Fig. 6b). The more dense SiO_2-structure of nanoparticle III as compared with the structure of nanoparticle IV leads to shifting of the Raman spectrum peaks towards higher frequencies. Not all the distinct peaks in the $J(\omega)$-spectra, obtained at 1500 K for nanoparticles III and IV, can reflect the fundamental frequencies of normal oscillations of atoms. For example, in the Raman spectrum of nanoparticle III, the third and fourth peaks can reflect the overtones of the representative frequency, defined by the second peak, to a locating accuracy of 4.3 and 0.3%, respectively. In the $J(\omega)$-spectrum of nanoparticle IV, the fifth peak can be determined accurate to 6.9% as an overtone of the third peak frequency.

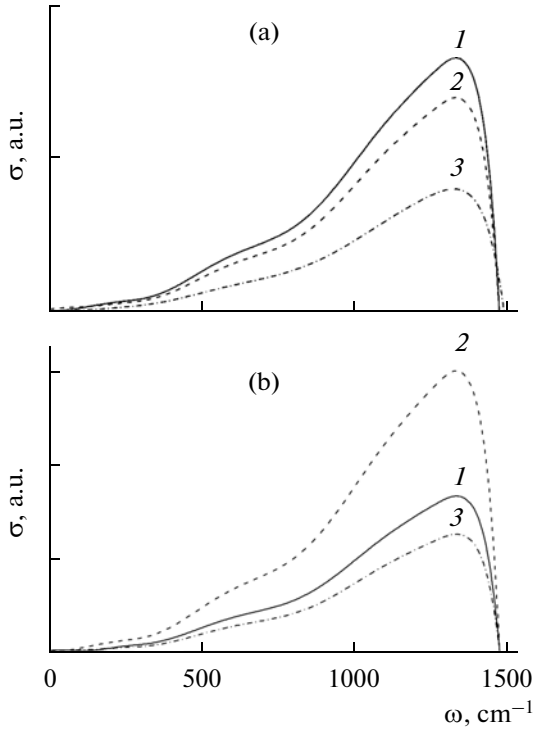

Fig. 4. The smoothed infrared absorption spectra for nanoparticles $(SiO_2)_{50}(GaAs)_{54}$ with SiO_2-core (a) and GaAs-core (b) at temperatures of *1*, 300 K; *2*, 900 K; *3*, 1500 K.

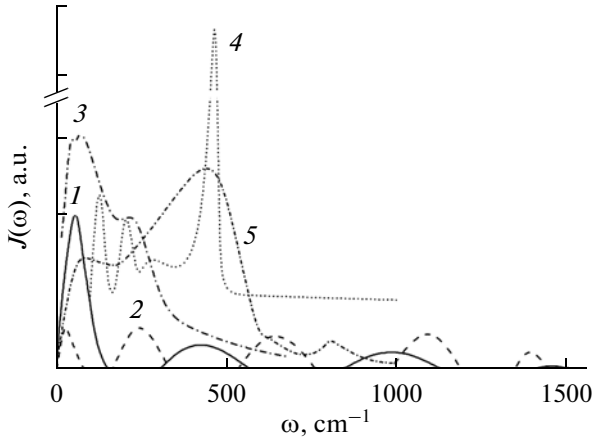

Fig. 5. The Raman spectra for various systems: *1*, nanoparticle III; *2*, nanoparticle IV; *3*, amorphous gallium, experiment [23]; *4*, α-quartz, experiment [24]; *5*, molten quartz, experiment [25].

The frequency dependences of the refraction index η and the absorption coefficient κ of nanoparticles III and IV are of the same type (Fig. 7). But the oscilla-

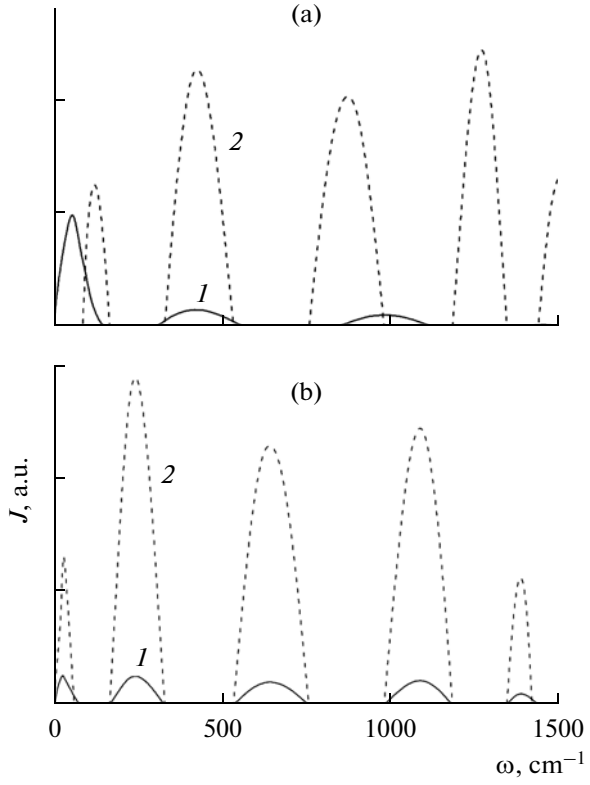

Fig. 6. The anti-Stokes spectra of Raman scattering for nanoparticles $(SiO_2)_{50}(GaAs)_{54}$ with SiO_2-core (a) and GaAs-core (b) at temperatures of *1*, 300 K; *2*, 1500 K.

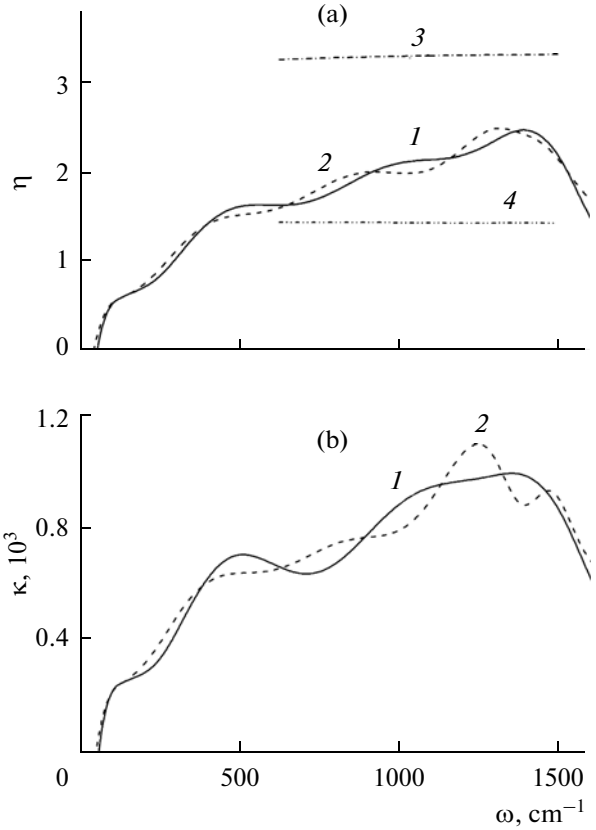

Fig. 7. The frequency dependence of refraction index (a) and absorption coefficient (b) for various systems: *1*, nanoparticle III; *2*, nanoparticle IV; *3*, crystal GaAs, experiment [27]; *4*, amorphous SiO_2, experiment [28].

tions of the η(ω) and κ(ω) functions are usually phase-shifted. The experimental values of the refraction index η of crystal GaAs [27] (line *3*) and amorphous silicon dioxide SiO_2 [28] (line *4*) in the frequency range of 700 to 1500 cm^{-1} form a band where the index η values for nanoparticles III and IV lie. The high-frequency oscillation of the κ(ω) function for nanoparticle III has a lower amplitude but longer duration than the analogous feature for nanoparticle IV.

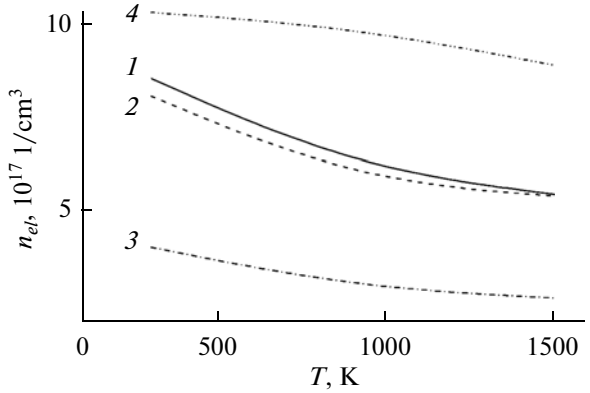

Fig. 8. The number of optically active electrons in nanoparticles: *1*, III; *2*, IV; *3*, I; *4*, II.

The number of electrons n_{el} involved in creating optical effects decreases as the nanoparticles heat (Fig. 8). Nanoparticle III (curve *1*) has higher values of n_{el} than nanoparticle IV. This is due to the location of Ga atoms near the nanoparticle surface. However, as the temperature rises, the difference in n_{el} values for nanoparticles III and IV smoothes and at $T = 1500$ K it almost disappears. The number of optically active electrons is distinctly higher for the GaAs nanoparticle and lower for SiO_2 particle than for four-component nanoparticles. Nanoparticle II has a descending convex plot $n_{el}(T)$ and nanoparticle I has a concave plot like four-component nanoparticles.

CONCLUSIONS

Progress in the synthesis of high-quality nanomaterials makes it possible to investigate one of the most fundamental issues concerning the influence of the size, structure, and surface of nanoparticles on their dynamic properties including the infrared and Raman spectra. Such investigations are necessary to gain better understanding of the basic physics of controlling

the parameters of nanoparticles in order to get the required dynamic properties, including the cases of thermal and mechanical load of nanoobjects.

In this paper the basic optical properties of two- and four-component nanoparticles of silicon dioxide and gallium arsenide at temperatures of 300 to 1500 K were studied. The integral intensity of the infrared absorption spectra of four-component nanoparticles decreases as temperature rises. But the structural relaxation of the SiO_2-coating of the GaAs-core can result in increasing the intensity of this part of the infrared spectrum despite the temperature rise. The shape of Raman spectra for these particles also depends strongly on the way the GaAs- and SiO_2-components are located in the nanoparticle. Increasing the temperature of $(SiO_2)_{50}(GaAs)_{54}$-nanoparticles causes a significant rise in the intensity of the anti-Stokes part of the Raman spectrum. Heating the nanoparticles to 1500 K does not lead to the shift of $J(\omega)$-spectrum peaks for the nanoparticle with SiO_2-coating, while the odd $J(\omega)$-spectrum peaks for the nanoparticle with the SiO_2-core shift in opposite directions. The refractive index and absorption coefficient depend weakly on the arrangement of the conductor (GaAs) and isolator (SiO_2) in the nanoparticle. The number of optically active electrons is also barely sensitive to the spatial inversion of a semiconductor and isolator in the nanoparticle formed from gallium arsenide and silicon dioxide.

Thus, using molecular-dynamic modeling, one can predict the significant optical properties of semiconductor particles having widespread application.

ACKNOWLEDGMENTS

This work was supported by the Presidium of the Ural Branch, Russian Academy of Sciences, and the Presidium of the Far East Branch, Russian Academy of Sciences, within the framework of integration project no. 09-C-2-1004, carried out at the Ural Branch, Russian Academy of Sciences, and the Far East Branch, Russian Academy of Sciences.

REFERENCES

1. Okuyama, K. and Lenggoro, I.W., *Chem. Eng. Sci.*, 2003, vol. 58, p. 537.
2. Vassileva, E. and Furuta, N., *Fresenius J. Anal. Chem.*, 2001, vol. 370, p. 52.
3. Kim, J.S., Kim, E.K., Song, J.D., Choi, W.J., and Lee, J.I., *J. Korean Phys. Soc.*, 2006, vol. 49, p. 2124.
4. Nordlund, K., Peltola, J., Nord, J., and Keinonen, J., *J. Appl. Phys.*, 2000, vol. 90, p. 1710.
5. Mitin, V.F., *Mol. Phys. Rep.,* 1998, vol. 21, p. 71.
6. Tersoff, J., *Phys. Rev. B*, 1989, vol. 39, p. 5566.
7. Tersoff, J., *Phys. Rev. Lett.*, 1986, vol. 56, p. 632.
8. Munetoh, S., Motooka, T., Moriguchi, K., and Shintani, A., *Comput. Mater. Sci.*, 2007, vol. 39, p. 334.
9. Nishidate, Y. and Nikishkov, G.P., *Comput. Model. Eng. Sci.*, 2008, vol. 26, p. 91.
10. Yasukawa, A., *Jpn. Soc. Mech. Eng.*, 1996, vol. 39, p. 313.
11. Benkabou, F., Certier, M., and Aourag, H., *Mol. Simul.*, 2003, vol. 29, p. 2001.
12. Kul'bachinskii, V.A., *Soros. Obraz. Zh.*, 2001, vol. 7, p. 98.
13. Le Bail, A., *J. Appl. Crystallogr.*, 2005, vol. 38, p. 389.
14. Galashev, A.E., *High Temp.*, 2012, vol. 50, no. 2, p. 204.
15. Galashev, A.E. and Rakhmanova, O.R., *Inzh.–Fiz. Zh.*, 2011, vol. 84, p. 1148.
16. Galashev, A.E., Rakhmanova, O.R., and Novruzova, O.A., *High Temp.*, 2011, vol. 49, no. 2, p. 193.
17. Galashev, A.E., Rakhmanova, O.R., and Novruzova, O.A., *High Temp.*, 2011, vol. 49, no. 4, p. 528.
18. *CRC Handbook of Chemistry and Physics*, Lide, D.R., Ed., 77th ed., Boca Raton, Florida: CRC Press, 1996.
19. Bosma, W.B., Fried, L.E., and Mukamel, S., *J. Chem. Phys.*, 1993, vol. 98, p. 4413.
20. Landau, L.D. and Lifshitz, E.M., *Course of Theoretical Physics: Volume 8. Electrodynamics of Continuous Media*, Oxford: Butterworth–Heinemann, 1984.
21. Tan, G.-L., Lemon, M.F., and French, R.H., *J. Am. Ceram. Soc.*, 2003, vol. 86, p. 1885.
22. Philipp, H.R. and Ehrenreich, H., *Phys. Rev.*, 1963, vol. 129, p. 1550.
23. Vilcarromero, J., Bustamante, R., and Silva, J.H.D., *Braz. J. Phys.*, 2006, vol. 36, p. 1035.
24. Ocana, M., Fornes, V., Garcia-Ramos, J.V., and Serna, C.J., *Phys. Chem. Miner.*, 1987, vol. 14, p. 527.
25. Bruckner, R., *J. Non-Cryst. Solids*, 1970, vol. 5, p. 123.
26. Berg, R.S., Mavalvala, N., and Steinberg, T., *J. Electron. Mater.*, 1990, vol. 19, p. 1323.
27. *Handbook of Optics*, Bass, M., Ed., New York: McGraw-Hill, 2010, vol. IV.
28. Malitson, I.H., *J. Opt. Soc. Am.*, 1965, vol. 55, p. 1205.